

Spex Young Star Atlas

We present a new spectral atlas of 46 young stars, compiled using a medium-resolution infrared spectrograph, SpeX, at the NASA Infrared Telescope Facility (IRTF) on Mauna Kea, Hawaii. SpeX maintains a resolution of $R \equiv \lambda/\Delta\lambda \sim 2000$, with a wavelength range of 0.70–2.55 μm . All atlas stars were selected from the star-forming region Upper Scorpius, which has a well-established age of ~ 11 Myr. Clear variations between old and young stars are observed, which will help constrain models of stellar evolution and atmospheres, at infrared wavelengths. Our new spectral atlas will allow for more accurate classification of young stars. Inconsistencies between infrared and optical spectral classifications will show the need for a more comprehensive young star library.

1. Introduction

Upper Scorpius (Upper Sco) is a star forming region located in the Scorpius-Centaurus Association. Members of star forming regions are born at approximately the same time. Upper Sco has an established age of ~ 11 Myr. Old stars are currently used in identifying spectral type Rayner et al. (2009); ?. With ages on the order of billions of years, these stars do not accurately represent young stars.

Observations made of young stars exhibit unexpected spectral features. These variations prove young stars need independent spectral classification. A stellar atlas of young stars does not exist at infrared (IR) wavelengths. IR observations cut through gas and dust found in star forming regions.

Presented here is an atlas of young stars, allowing for more accurate classification. Criteria required in building such an atlas is discussed in Section 2.1. This atlas will allow for the refinement of stellar evolution and atmosphere models. Doing so will allow for more accurate spectral classification of young stars.

[young star - surface gravity?]
[why ir wavelength]
[future prospects]

2. Observations and Data Reduction

2.1. Sample Selection

We selected 46 members of the Upper Scorpius star forming region spanning spectral types from M–O. Prior to observation, each target was vetted using the following criteria. Stars identified to have binary companions ? or accretion disks ?, were eliminated from the target list.

Restricting target objects based on such criteria ensures each observed spectra was as isolated and representative as possible.

To select potential targets, previously established spectral classes were used. Observations at optical wavelengths established spectral types, listed in Table 1.

2.2. Observations

All of the objects discussed in this paper were observed between March 2012 and June 2015 (Table 1), with the NASA Infra-Red Telescope Facility (IRTF) and the SpeX instrument Rayner et al. (1998). We used the short-wavelength cross-dispersed mode (SXD) with $R2000$ matched to $0.3 \times 15''$ slit. SpeX was upgraded in August 2014¹. This upgrade increased the observable wavelength range, filled in the gap around $1.8\mu\text{m}$, and increased SpeX’s wavelength sampling rate, allowing for higher accuracy of collected data. A portion of the objects in this catalog were observed prior to this upgrade. For this reason, it is necessary to compare data taken with each version of SpeX (Table 1), shown in Figure 2.

GSC 06801–00186 was observed on June 29, 2012 UT, before SpeX was upgraded, and again on June 15, 2015, after uSpeX was implemented[?]. Spectra collected after the upgrade span a larger wavelength range, but both SpeX and uSpeX data sufficiently cover the wavelength range needed for our study. Data collected with both versions follow the same procedure, discussed below. Before the upgrade, the wavelength range spanned $0.80\text{--}2.4\mu\text{m}$. Following August 2014, the wavelength range was expanded to span $0.70\text{--}2.55\mu\text{m}$.

During observations, integration times were altered as to maximize the Signal to Noise ratio (SNR). Observations were made in AB pairs. After the initial A frame is taken, the telescope offsets (“nods”) and captures a B frame. Both frames are of the the same science target, at a different position along the slit. Since our objects were treated as point sources, this AB mode allowed for the subtraction of the B frame from the A frame, leaving both positive and negative spectrum along with sky residuals Cushing et al. (2004). Subtraction of these pairs allows for the removal of dark currents and sky residuals.

After collecting data on a particular science object, flat and arc calibration frames were taken. In order to minimize the time between target observations and the collection of calibration frames, the telescope remained unmoved. Background noise was identified and removed using darks and flats.

Standard A0V stars also needed to be observed, for telluric line corrections. Which A0V to observe was determined by location and airmass. For our purposes, an ideal A0V would deviate

¹See http://irtfweb.ifa.hawaii.edu/~spex/SpeX_manual_06mar15.pdf for details.

from the science objects’ airmass by no more than 0.15 and be located in the same region of the sky as the science object. This ensured minimal atmospheric derivations between our science and A0V stars.

Effective temperatures with no identifying symbol come from from ?. A least-squares fit to published values allowed for determination of temperatures for unlisted spectral types. Only values pertaining to specific luminosity classes were used in each fit.

2.3. Data Reduction

For reduction of collected spectra, Spextool was used Cushing et al. (2004). Calibration frames consist of flats, arcs, and A0V standards. Flat frames allow for the removal of inconsistencies, amongst the detector’s pixels. Observations of an arc lamp permitted wavelength calibration. The choice of A0V stars as standards was based on their relatively few spectral features, outside hydrogen lines; making isolation of telluric lines significantly cleaner. For telluric reduction, an observed A0V star was compared to Vega. Deviations of the observed star, from the standard, are attributed to atmospheric interference. The same atmospheric disturbances apply to all objects observed at the same time and airmass. Telluric corrections were accomplished using spectroscopic observations of standard stars. B–V data, provided by Simbad ?, was used in in the standard selection process. In order to properly scale emission lines and account for velocity shifts, a kernel was constructed using the observed A0V. Finally, all orders were scaled and merged, producing a continuous spectrum. A more detailed account of this process is outlined by Vacca Vacca et al. (2003).

To be transformed from an array into a workable spectrum Spextool Cushing et al. (2004) was used. Once extracted, each spectra was visually reviewed. Hot pixels, outliers, and areas of low SNR were masked and removed. Through this process, the intrinsic spectrum of each star was better revealed. SNR calculations occurred between 2.025–2.162 μm . All stars in this sample have SNR above 95.

3. Data and Analysis

3.1. The Spectra

[See commented-out list above]

Spectral types listed in Table 1 were pulled from the literature. Spectral type references are identified by numbers, in the reference column of Table 1. For the 9 stars with multiple spectral references, each spectra was visually examined and compared to other spectra of the same class,

from existing libraries. References were chosen based on EW values and comparison of spectral features.

[**section 3.1 Rayner**]

[Digital copies of the spectra, with associated information, can be found at – – –.]

[Each spectra is available as a fits or png file.]

[Discuss masking of telluric regions.]

Table 2: EW Limit Definitions².

Feature	Feature Limits (μm)	First Continuum Level Limits (μm)	Second Continuum Level Limits (μm)
Ca II (0.866 μm)	0.8655–0.8673	0.862–0.864	0.870–0.873
Na I (1.14 μm)	1.137–1.1428	1.125–1.130	1.150–1.160
Al I (1.313 μm)	1.3118–1.3165	1.305–1.309	1.320–1.325
Mg I (1.485 μm)	1.4867–1.4895	1.4775–1.485	1.491–1.497
Mg I (1.711 μm)	1.7098–1.7130	1.702–1.708	1.715–1.720
Na I (2.206 μm)	2.204–2.211	2.192–2.198	2.213–2.220

3.2. Equivalent Widths

Following the procedure described by Cushing et al. (2005), Equivalent width (EW) values and variances, σ_{EW}^2 , are given by

$$EW = \sum_{i=1}^n \left[1 - \frac{f(\lambda_i)}{f_c(\lambda_i)} \right] \Delta\lambda_i, \quad (1)$$

$$\sigma_{EW}^2 = \sum_{i=1}^n \Delta\lambda_i^2 \left[\frac{\sigma^2(\lambda_i)}{f_c^2(\lambda_i)} + \frac{f^2(\lambda_i)}{f_c^4(\lambda_i)} \sigma_c^2(\lambda_i) \right], \quad (2)$$

C)

where $f(\lambda_i)$ and $f_c(\lambda_i)$ are the observed and estimated continuum flux densities, respectively. Uncertainties in the observed and estimated continuum flux densities, $\sigma(\lambda_i)$ and $\sigma_c(\lambda_i)$, were calculated following the procedure of Sembach & Savage (1992). $\Delta\lambda$ is the difference between subsequent wavelength intervals; $\Delta\lambda = \lambda_{i+1} - \lambda_i$. To preserve dimensionality, λ_n was appended to the end of each wavelength array, such that $\lambda_n = \lambda_{n+1}$.

²Table 8 of Rayner et al. (2009).

Rather than subtracting adjacent intervals, Sembach & Savage (1992) converted from wavelength to velocity-space and defined $d\nu = \nu_{i+\frac{1}{2}} - \nu_{i-\frac{1}{2}}$. Validation of these procedures was accomplished by calculating EW values and uncertainties of existing spectral libraries³. Calculated and published results were compared, showing both methodologies produce the same results.

³Table 9 of Rayner et al. (2009).

D)

 where $f(\lambda_i)$ and $f_c(\lambda_i)$ are the observed and estimated continuum flux densities, respectively. Uncertainties in the observed and estimated continuum flux densities, $\sigma(\lambda_i)$ and $\sigma_c(\lambda_i)$, were calculated following the procedure of Sembach & Savage (1992). After converting from wavelength to velocity-space, Sembach & Savage (1992) defined $d\nu = \nu_{i+\frac{1}{2}} - \nu_{i-\frac{1}{2}}$. Here, $\Delta\lambda$ is the difference between subsequent wavelength intervals; $\Delta\lambda = \lambda_{i+1} - \lambda_i$. To preserve dimensionality, λ_n was appended to the end of each wavelength array, such that $\lambda_{n+1} = \lambda_n$. Validation of this procedure was accomplished by calculating EW and σ_{EW} for stars in existing spectral libraries⁴. Once calculated, results were compared to published values. Within error, both methods produce the same results.

Spectral features act as indicators of many stellar properties. The absorption lines listed in Table 2 can be used to determine spectral types of cool stars Rayner et al. (2009). Equivalent width (EW) values of these features are given in Table 3.

Look at commented out lists above...and Discuss:

- which lines were chosen and why
- how do the lines map to spt type...lum class
- what features are for young stars?

4. Comparison with Models

5. Needed Citations

Sample Selection section

- NEED NAME OF PERSON WHO COMPLETE BINART SURVEY - DAVID L (GEMINI)?
- NEED NAME OF PERSON WHO COMPLETED ACCRETION DISK SURVEY

Observation section

- Rayner et al. (2003)

⁴Table 9 of Rayner et al. (2009).

- cite whomever was referenced as identifying binaries ?
- cite whomever was referenced as identifying accretion disks Carpenter et al. (2006)
- when upgrade of Spex occurred ?
- ?

Data Reduction and Analysis section

- Lord, S. D., 1992, NASA Technical Memorandum 103957
- Gemini Observatory for telluric transmission regions shown in gray on plots
- Simbad

5.1. From Adam Kraus

G, K, and early M stars: Kohler et al. (2000), Kraus et al. (2008), Lafreniere et al. (2014)

Mid/late M stars: Kraus et al. (2005), Bouy et al. (2006), Biller et al. (2011), Kraus & Hillenbrand (2012)

For disks, it's a little simpler. You can just use Carpenter et al. (2006, 2009) and Luhman & Mamajek (2012). test

REFERENCES

- Carpenter, J., Hillenbrand, L., Mamajek, E., Meyer, M., & Slesnick, C. 2006, Circumstellar Disks in the Upper Scorpius OB Association, Spitzer Proposal
- Cushing, M. C., Rayner, J. T., & Vacca, W. D. 2005, ApJ, 623, 1115
- Cushing, M. C., Vacca, W. D., & Rayner, J. T. 2004, PASP, 116, 362
- Rayner, J. T., Cushing, M. C., & Vacca, W. D. 2009, ApJS, 185, 289
- Rayner, J. T., Toomey, D. W., Onaka, P. M., et al. 2003, Publications of the Astronomical Society of the Pacific, 115, 362
- Rayner, J. T., Toomey, D. W., Onaka, P. M., et al. 1998, in Proc. SPIE, Vol. 3354, Infrared Astronomical Instrumentation, ed. A. M. Fowler, 468–479
- Sembach, K. R., & Savage, B. D. 1992, ApJS, 83, 147

Vacca, W. D., Cushing, M. C., & Rayner, J. T. 2003, Publications of the Astronomical Society of the Pacific, 115, 389

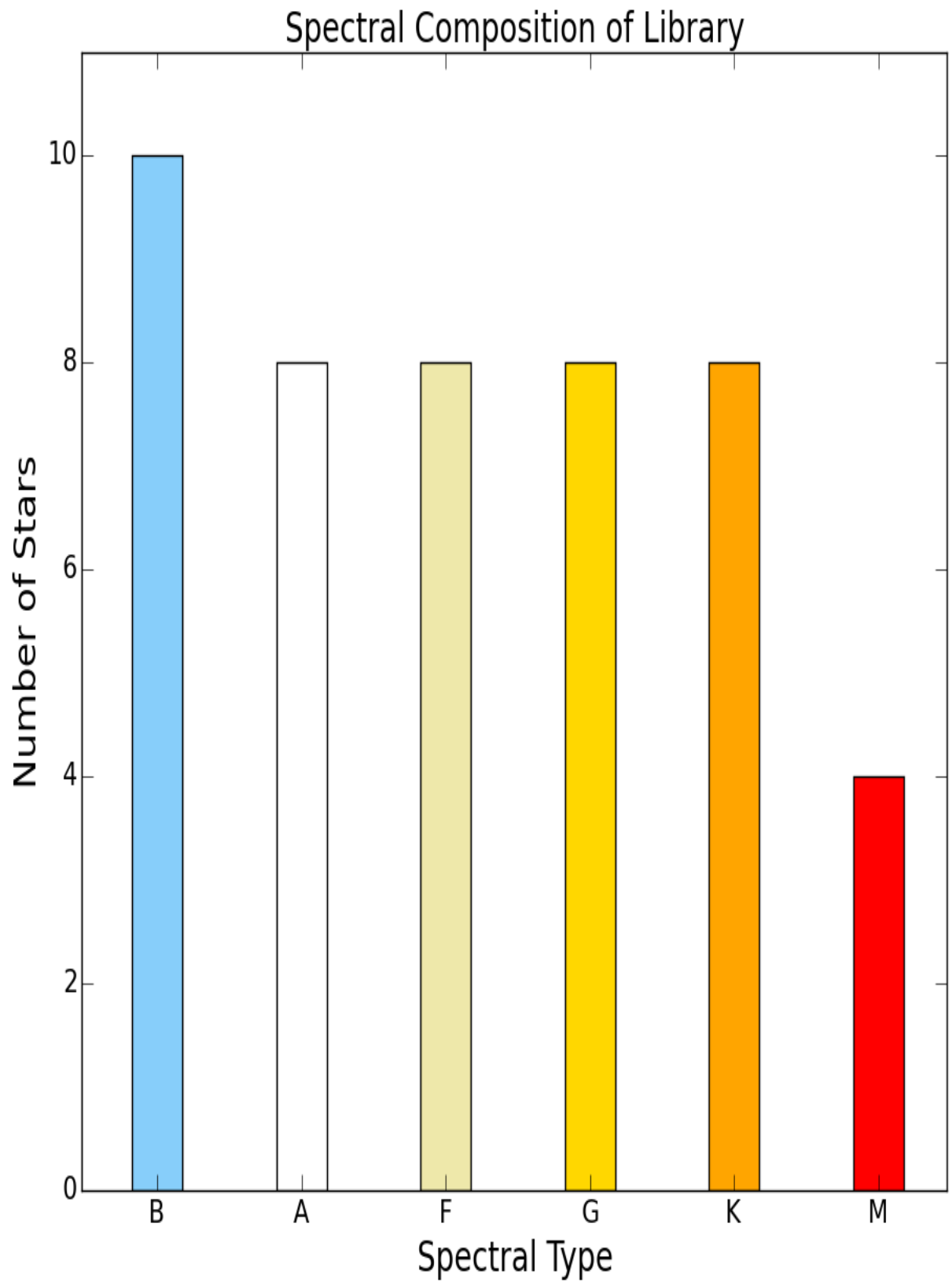
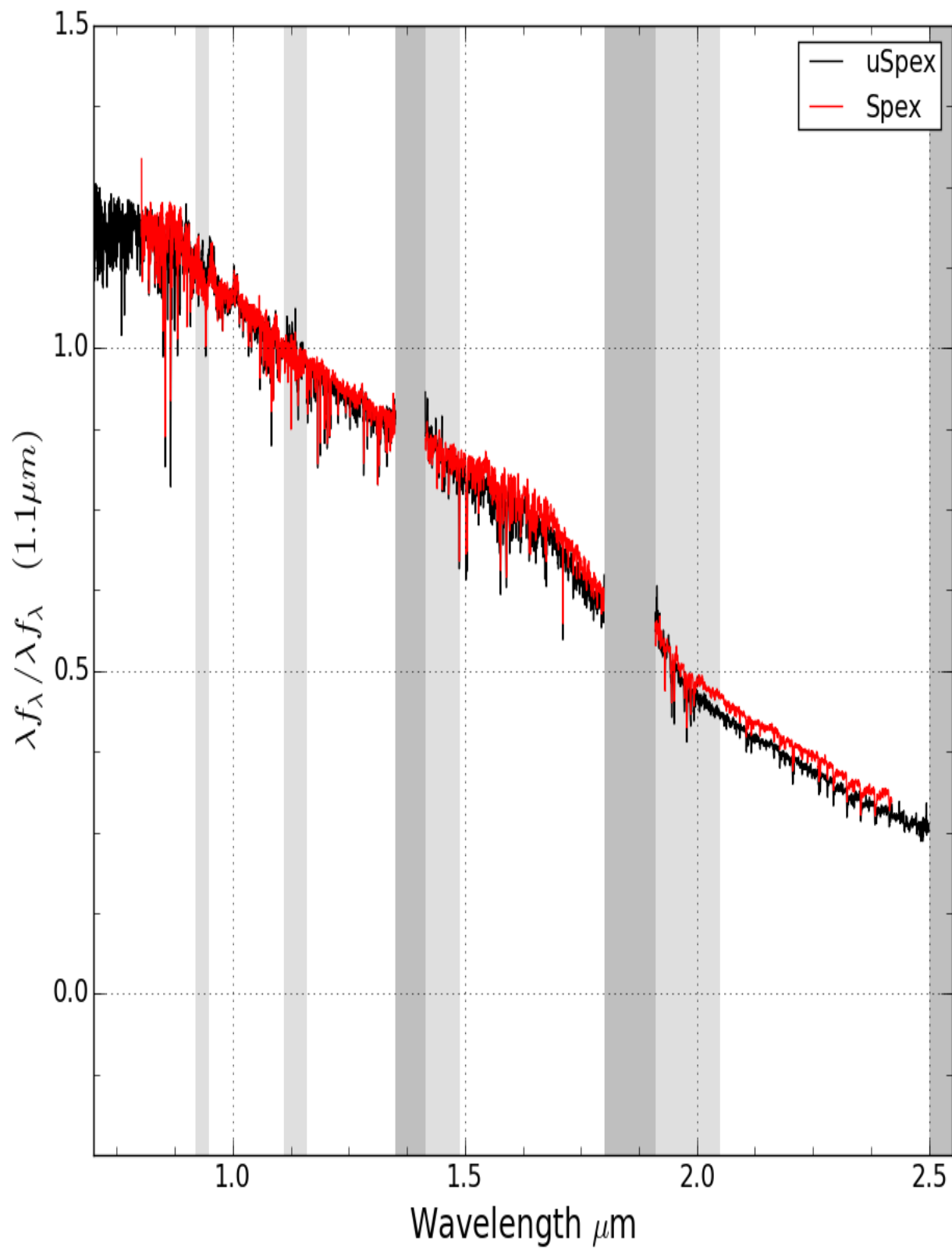
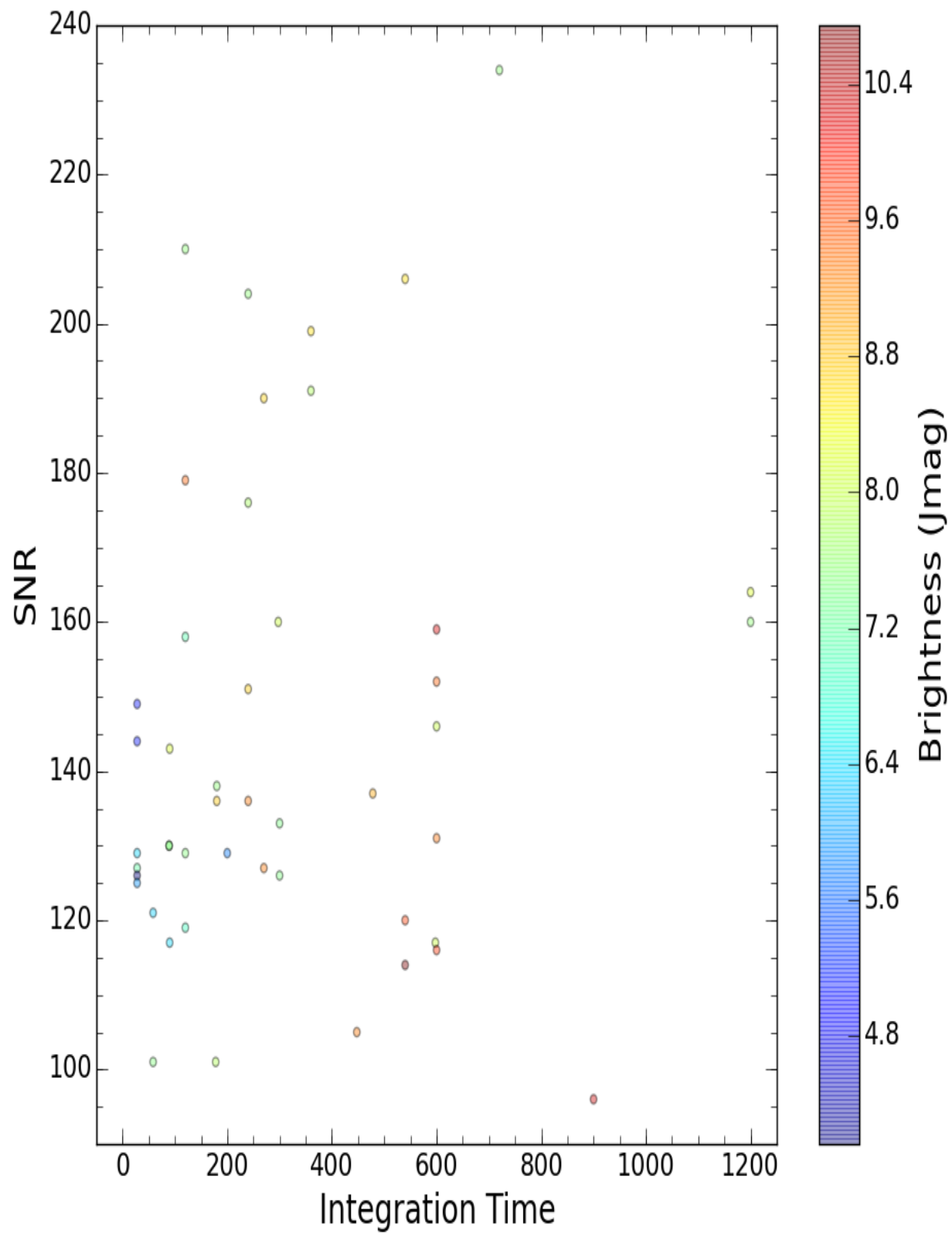
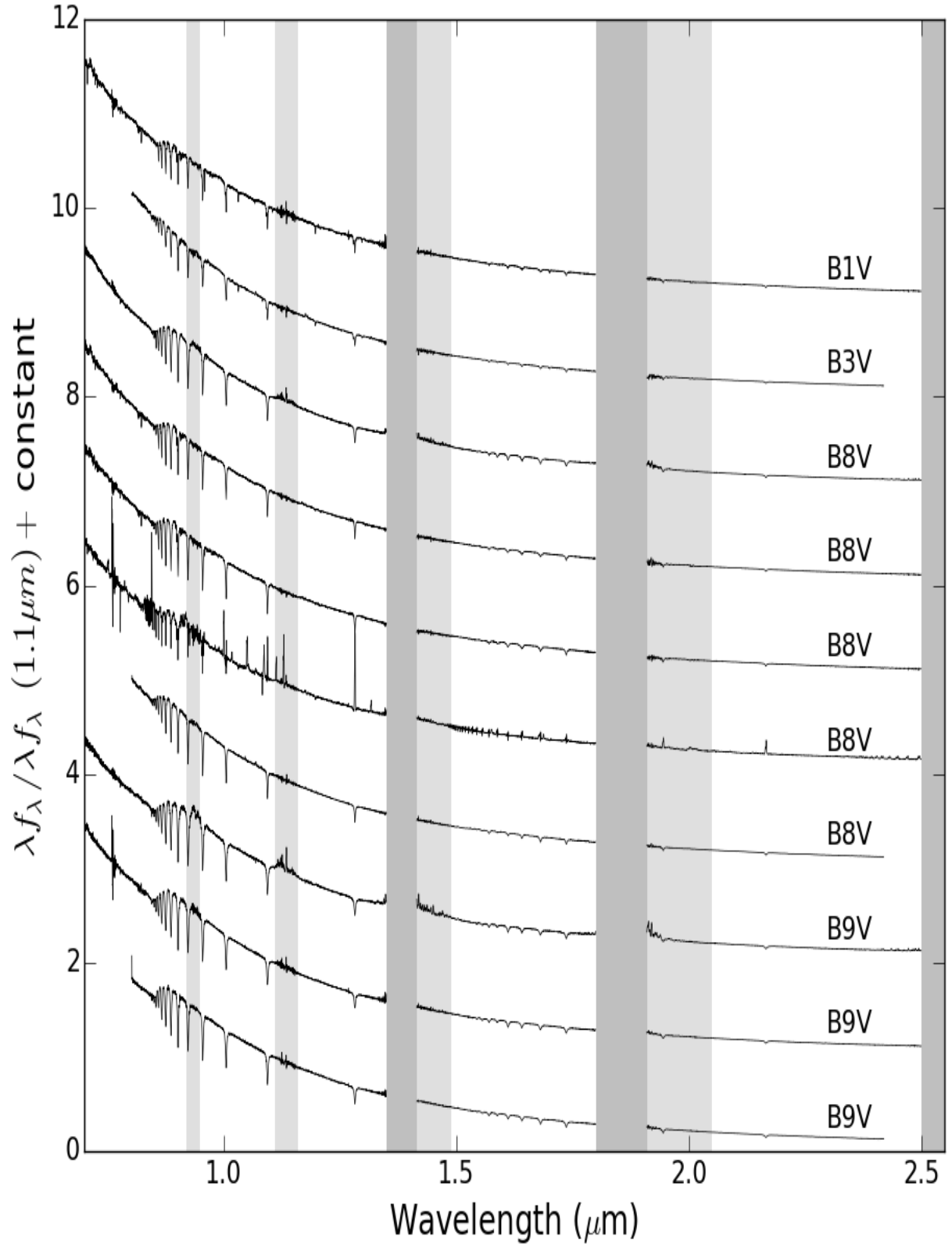


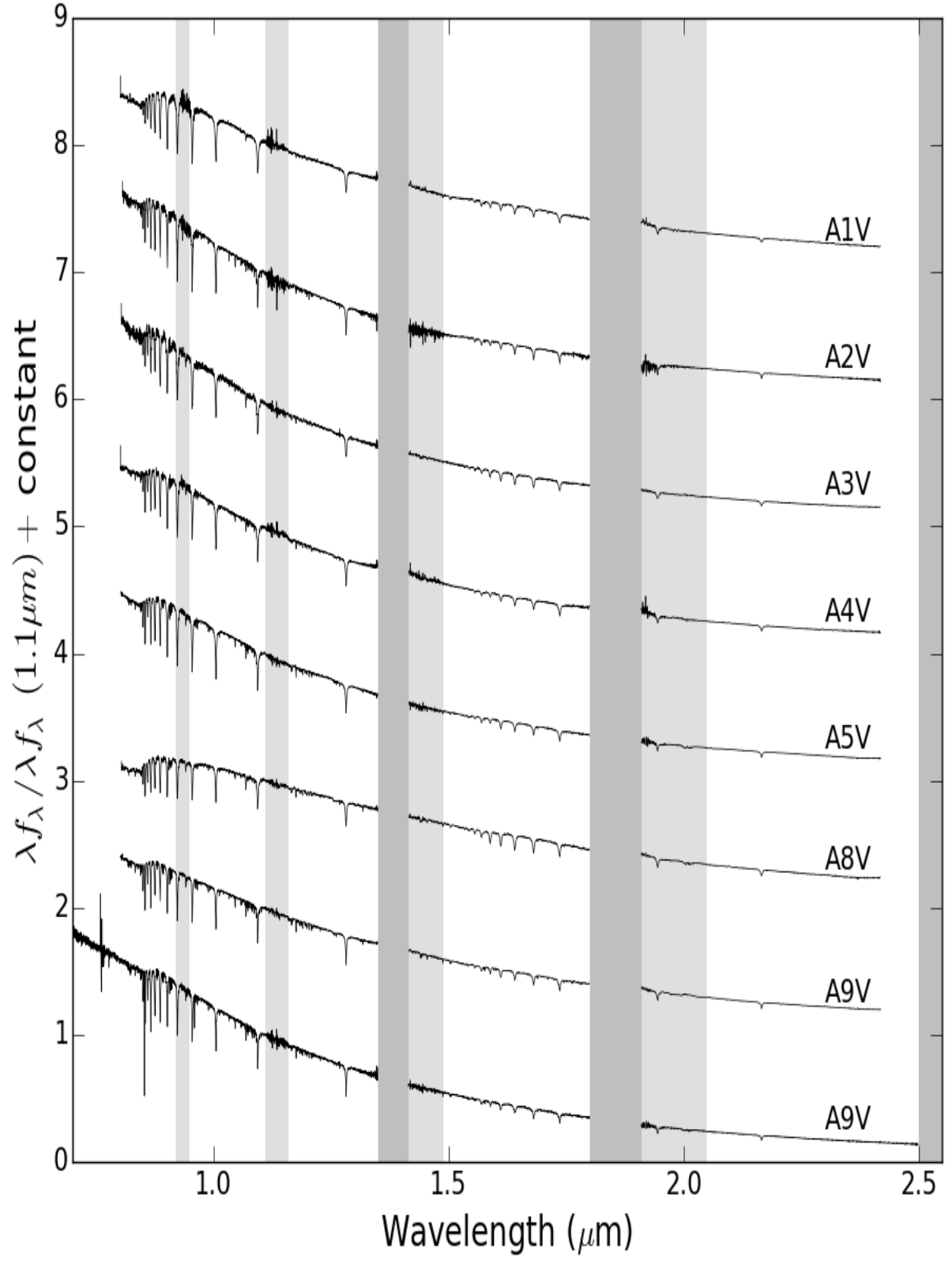
Table 1: Listed here are observed targets with corresponding information.

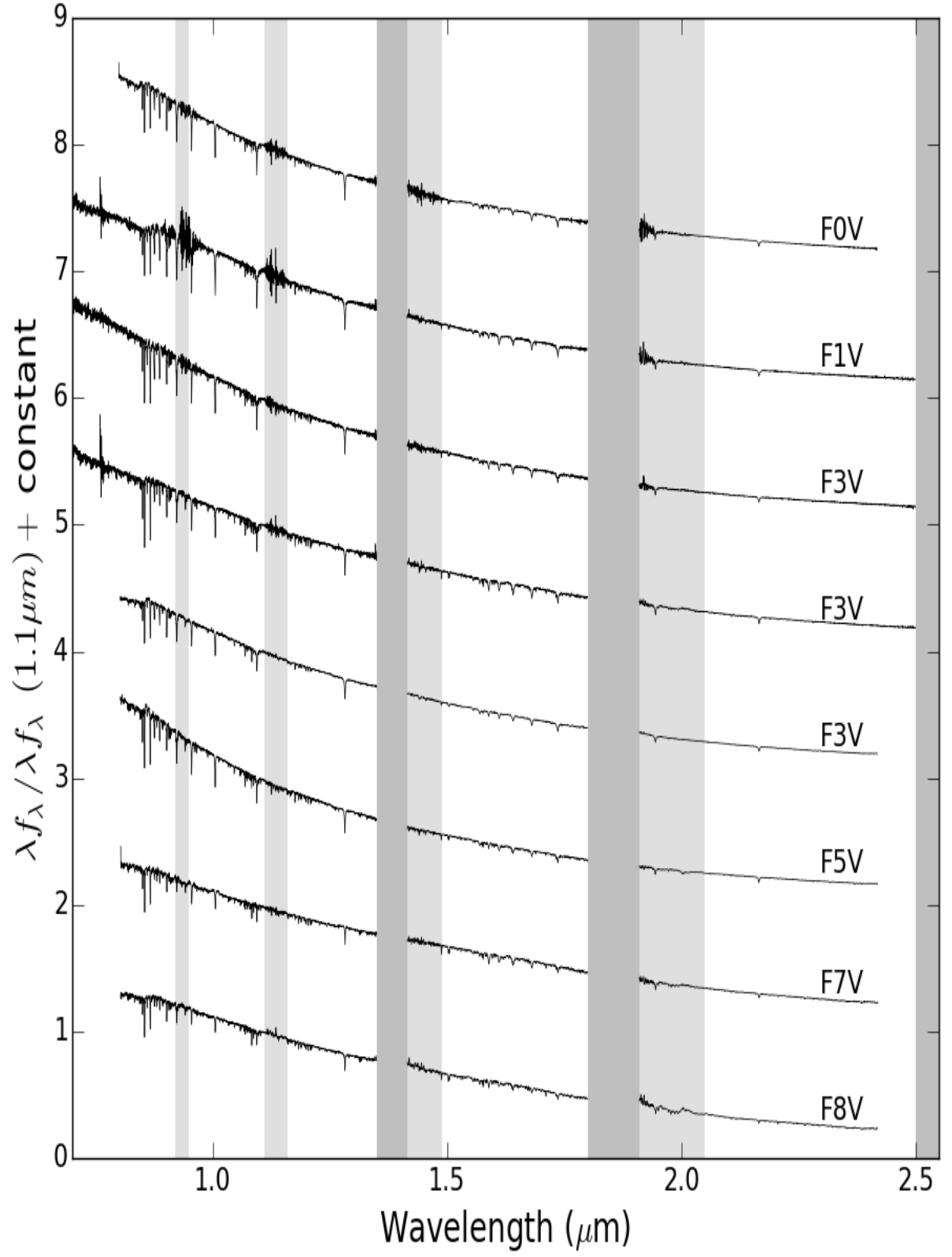
Object	RA	DEC	Lit. Spectral Type	UT Date	J (mag)	SNR	Total
HD 146266	16:16:23.32	-25:03:49.1	A1V	7/18/2012	7.533	210	
HD 143472	16:01:26.93	-25:11:56.6	A2V	7/18/2012	7.074	158	
HD 145468	16:11:52.96	-22:32:42.1	A3V	6/29/2012	7.45	126	
HD 142424	15:55:17.16	-23:22:17.4	A4V	7/18/2012	7.54	138	
HD 142097	15:53:21.87	-21:58:20.6	A5V	7/12/2012	7.493	129	
HD 146899	16:19:38.05	-26:52:31.6	A8V	6/29/2012	8.569	206	
HIP 73990	15:07:14.53	-29:30:01.5	A9V	6/15/2015	7.499	130	8
HD 147137	16:20:50.48	-22:35:45.2	A9V	7/12/2012	8.032	146	
HIP 78933	16:06:48.64	-20:40:02.7	B1V	6/15/2015	4.16	126	2
HD 144470	16:06:48.96	-20:40:14.4	B1V	7/12/2012	4.16	44	
HD 138485	15:32:55.67	-16:51:16.5	B3V	7/12/2012	5.78	129	
HD 147196	16:21:19.54	-23:42:34.9	B6/B7Vn	7/12/2012	6.565	16	
HIP 70753	14:28:10.35	-29:29:26.1	B8V	6/15/2015	5.073	149	2
HIP 77909	15:54:38.54	-25:14:42.4	B8V	6/15/2015	5.925	125	2
HIP 79031	16:07:51.15	-24:27:47.7	B8V	6/15/2015	6.379	129	2
HIP 78207	15:58:11.48	-14:16:40.6	B8V	6/15/2015	5.098	144	2
HD 144661	16:07:51.99	-24:27:42.8	B8V	7/18/2012	6.379	117	
HIP 76633	15:39:00.11	-19:43:50.9	B9V	6/15/2015	7.476	101	5
HIP 79599	16:14:28.97	-21:06:20.4	B9V	6/15/2015	6.342	121	5
HD 143567	16:01:55.60	-21:58:50.4	B9V	7/18/2012	6.928	119	
HD 137130	15:25:08.91	-26:34:30.9	F0V	3/22/2012	7.566	160	1
HIP 79369	16:11:55.19	-21:06:10.4	F1V	6/15/2015	7.855	101	1
HIP 82319	16:49:10.74	-22:42:46.5	F3V	6/15/2015	8.05	117	5
HD 146743	16:18:39.41	-21:35:39.6	F3V	7/12/2012	7.838	191	
HD 148153	16:27:12.68	-27:11:27.2	F5V	7/12/2012	7.419	133	
HIP 78977	16:07:17.56	-22:03:39.8	F7V	6/29/2012	7.543	204	
HIP 71982	14:43:19.42	-10:35:13.5	F8V	6/15/2015	7.474	130	8
HD 142113	15:53:21.17	-19:23:58.8	F8V	7/12/2012	7.782	176	
HIP 61412	12:35:00.73	-26:42:46.3	G0V	6/15/2015	7.162	127	2
HD 148040	16:26:29.32	-27:41:17.0	G0V	3/22/2012	7.554	234	
HD 133748	15:06:51.76	-23:37:27.6	G2V	3/22/2012	8.251	164	1
GSC 06793-00994	16:14:02.15	-23:01:08.0	G4V	7/12/2012	9.375	131	
HBC 649	16:34:09.09	-15:48:01.4	G5V	6/15/2015	8.995	137	4
GSC 06801-00186 (oldSpx)	16:14:59.03	-27:50:27.1	K0IV(e)	6/29/2012	9.334	136	
GSC 06801-00186	16:14:59.30	-27:50:17.9	K0IV(e)	6/15/2015	9.334	105	4
GSC 06793-01406	16:16:17.80	-23:39:51.3	G7V	6/29/2012	8.727	151	
GSC 06213-00306AB	16:13:18.19	-22:12:52.3	G9V	6/29/2012	8.18	143	
CD-25 11942	17:06:00.85	-25:20:25.9	K0V	6/15/2015	8.099	160	2
ScoPMS 214	16:29:48.69	-21:52:17.2	K0 / K2IV(e)	7/12/2012	8.677	190	
HD 141813	15:51:54.35	-26:22:09.2	K0 / K1III+	7/12/2012	8.232	30	
HD 14311	15:58:57.31	-13:10:14.3	K0III	7/12/2012	7.263	62	
ScoPMS 44	16:11:08.86	-19:04:51.8	K2 / K2IV(e)	7/12/2012	8.761	136	
GSC 06793-00797	16:13:02.68	-22:57:49.2	K4V	6/29/2012	9.322	127	

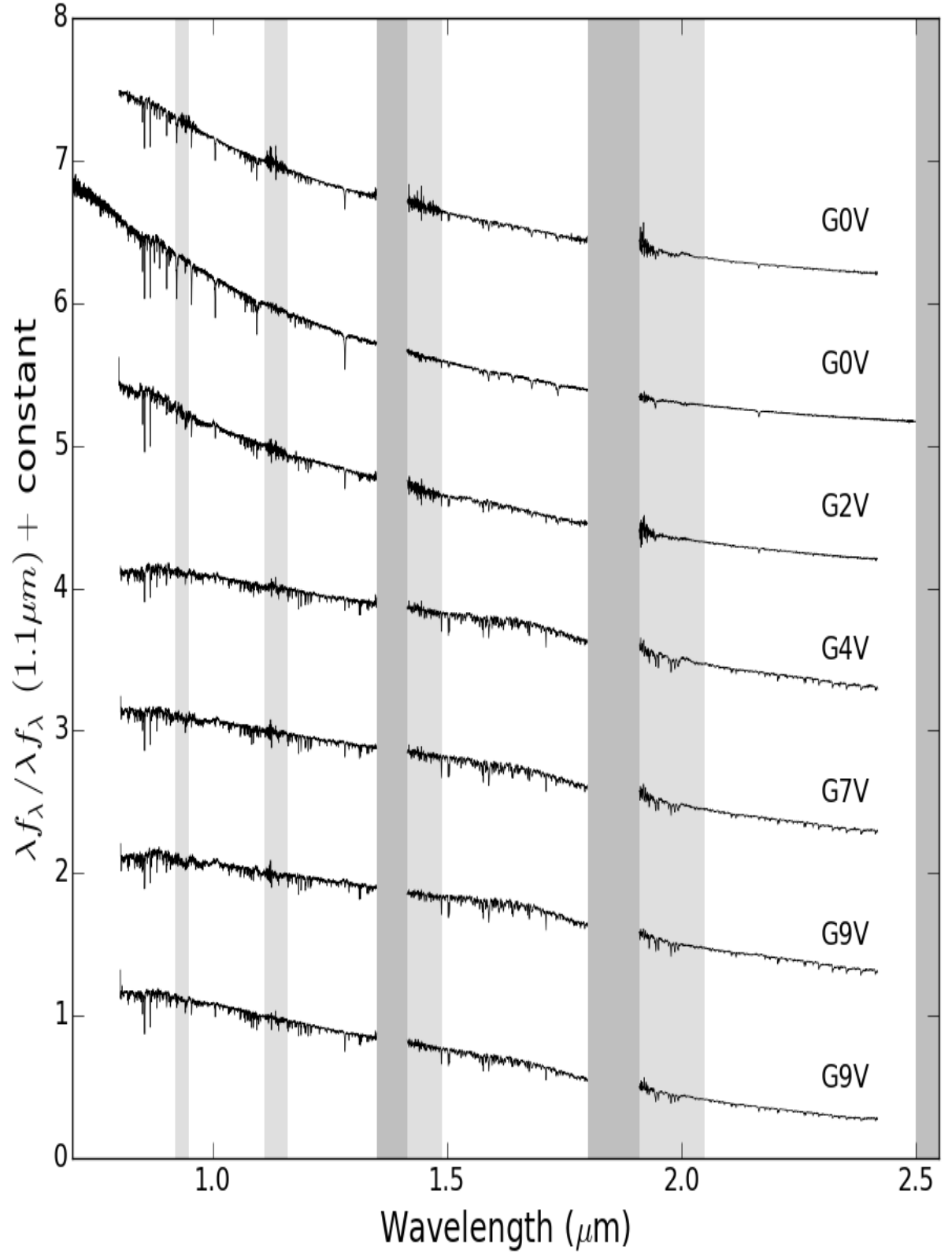


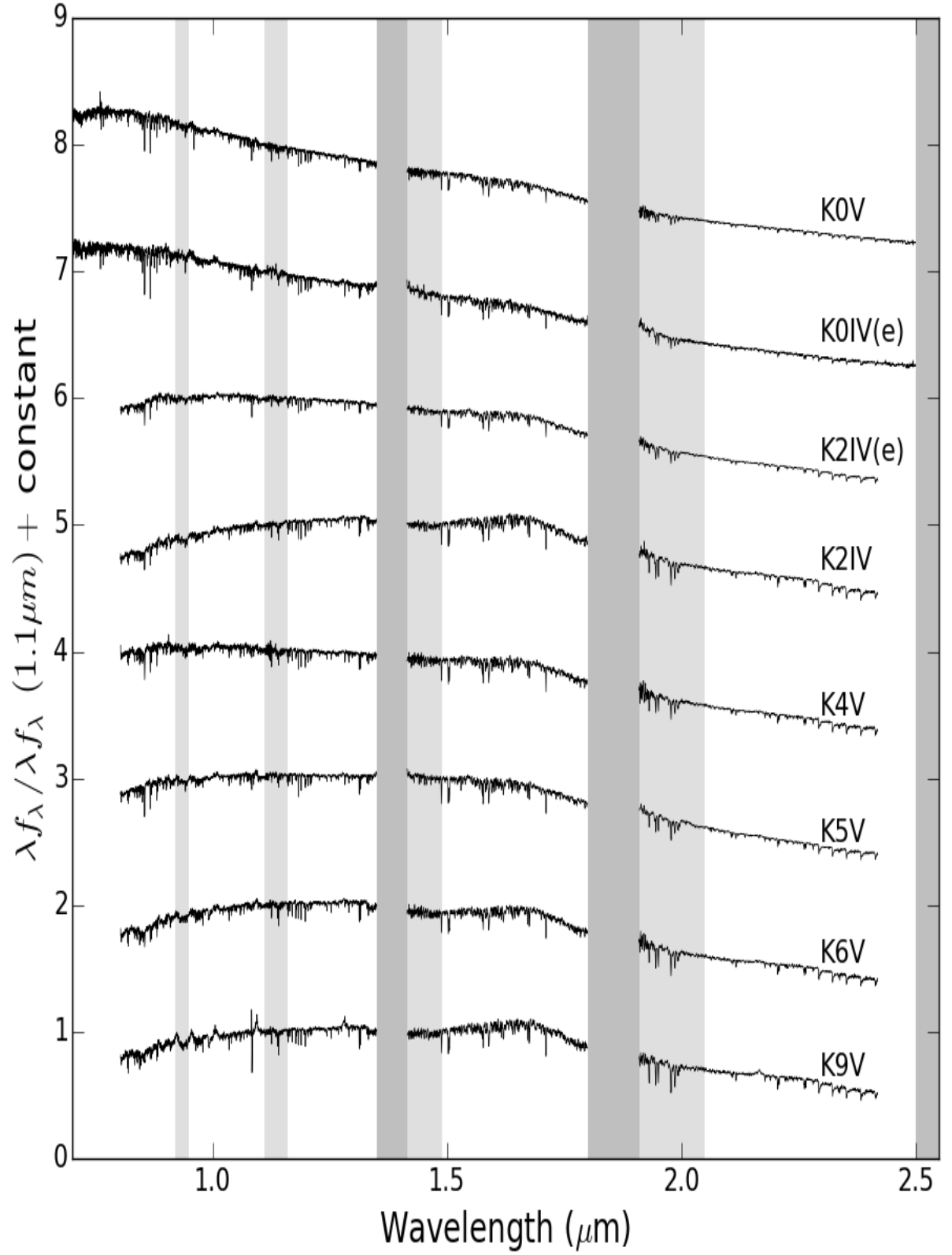


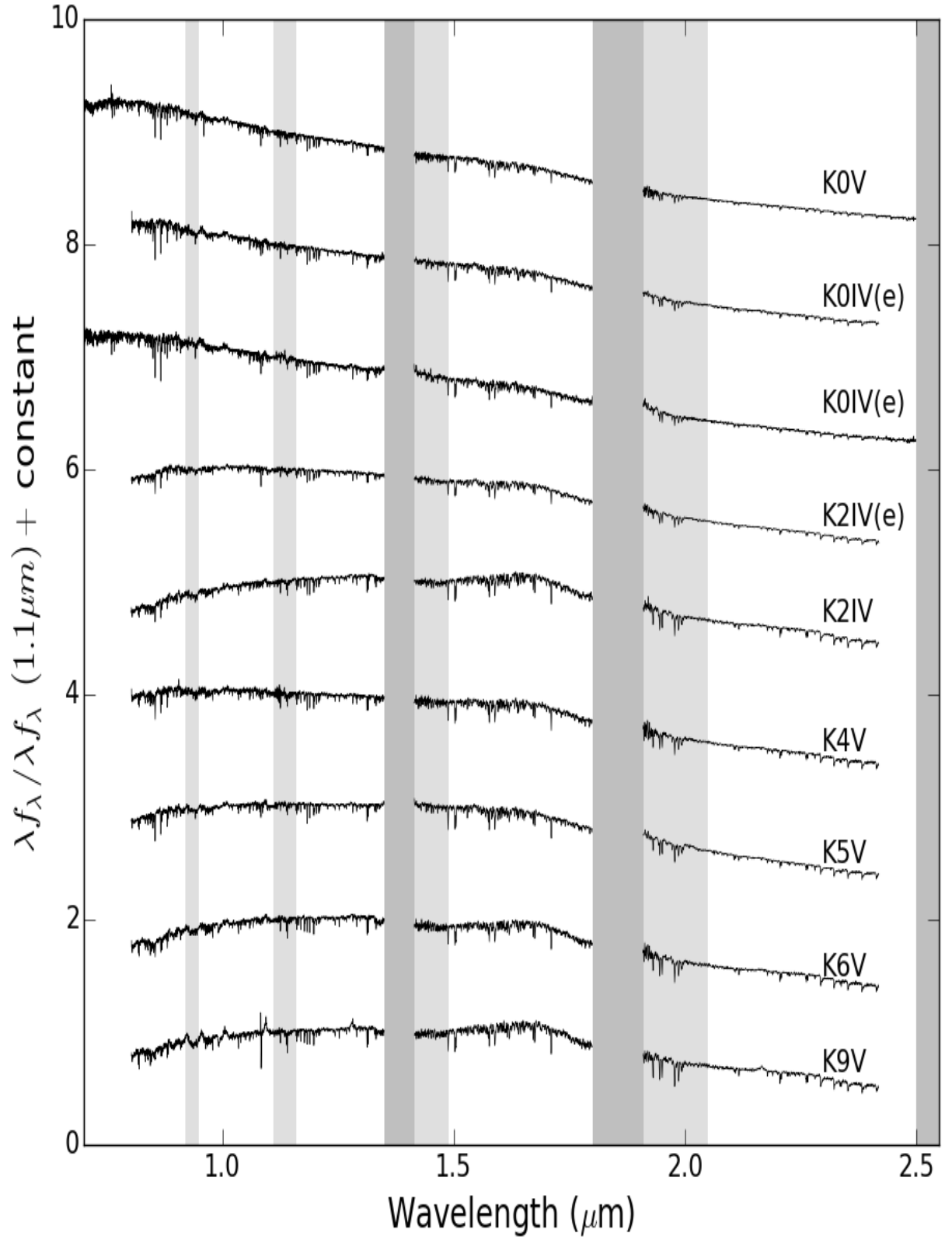


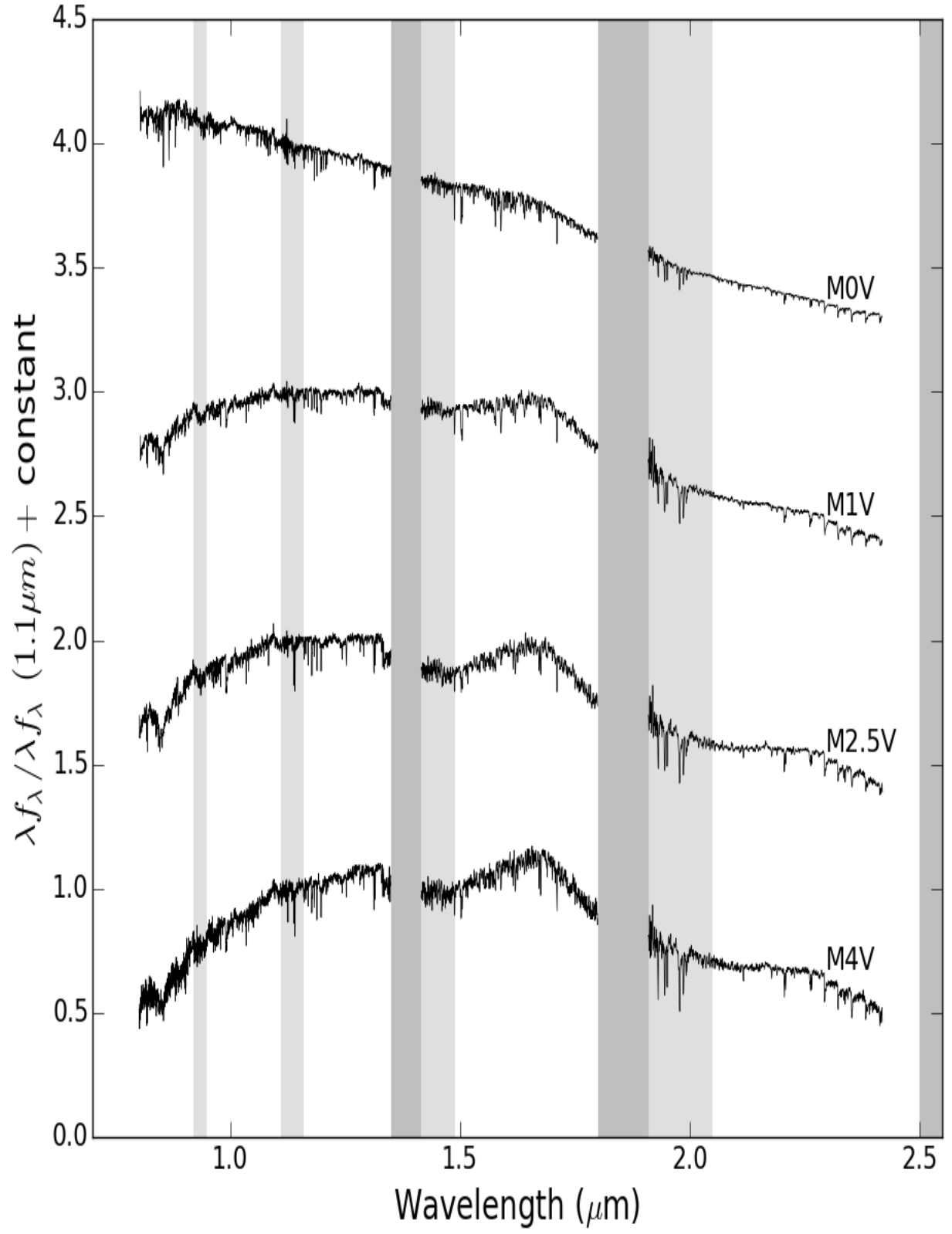


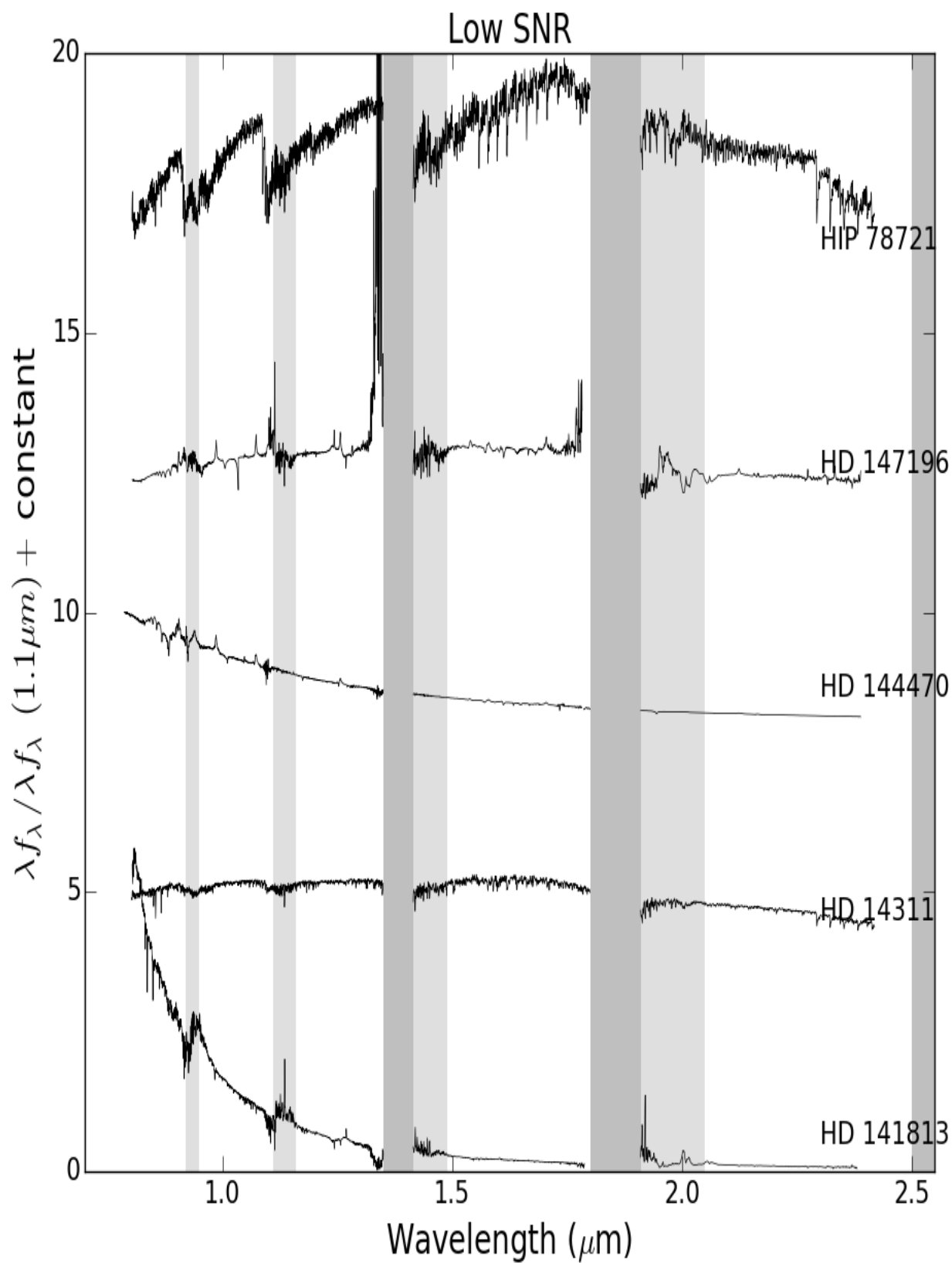


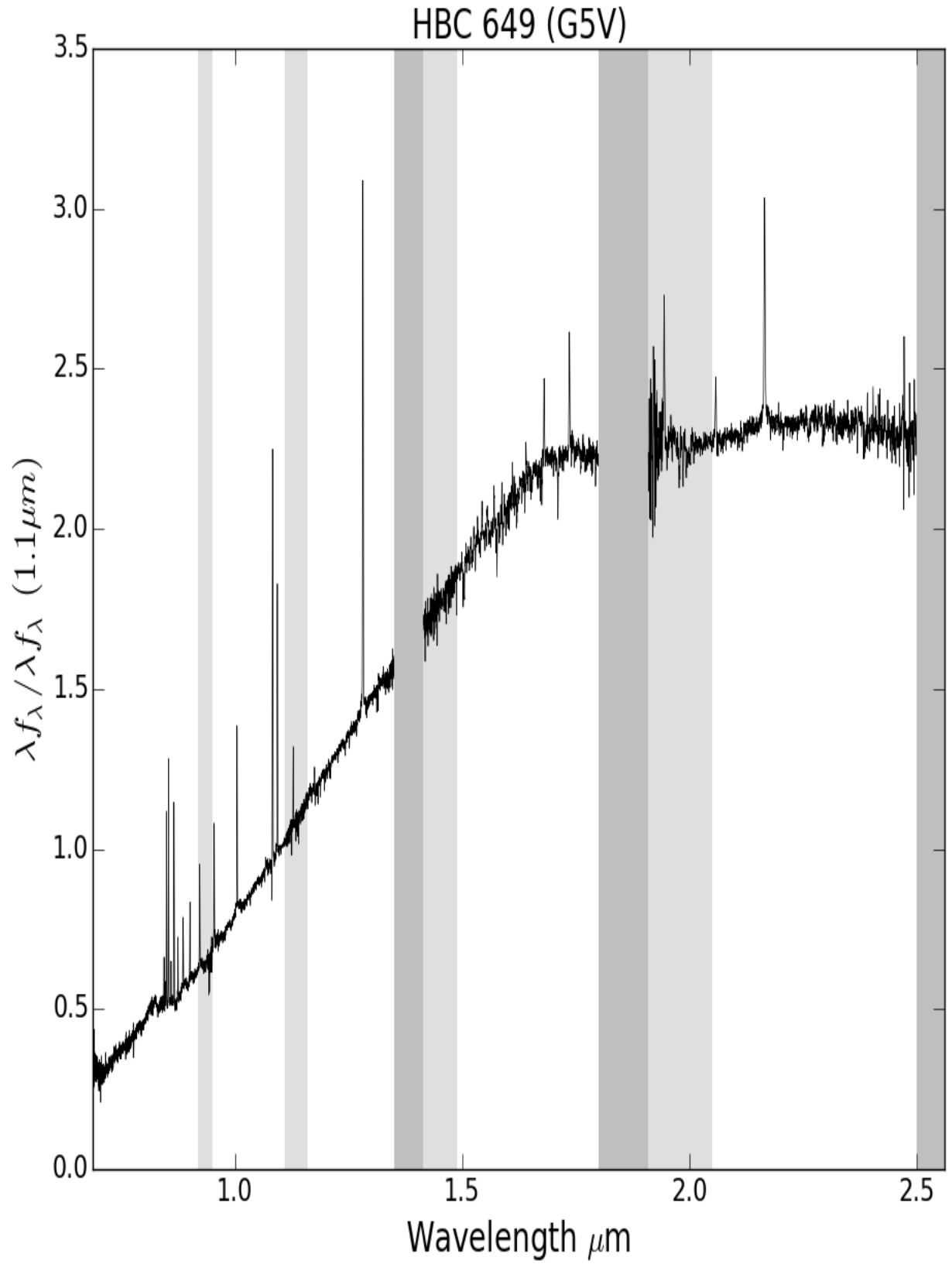


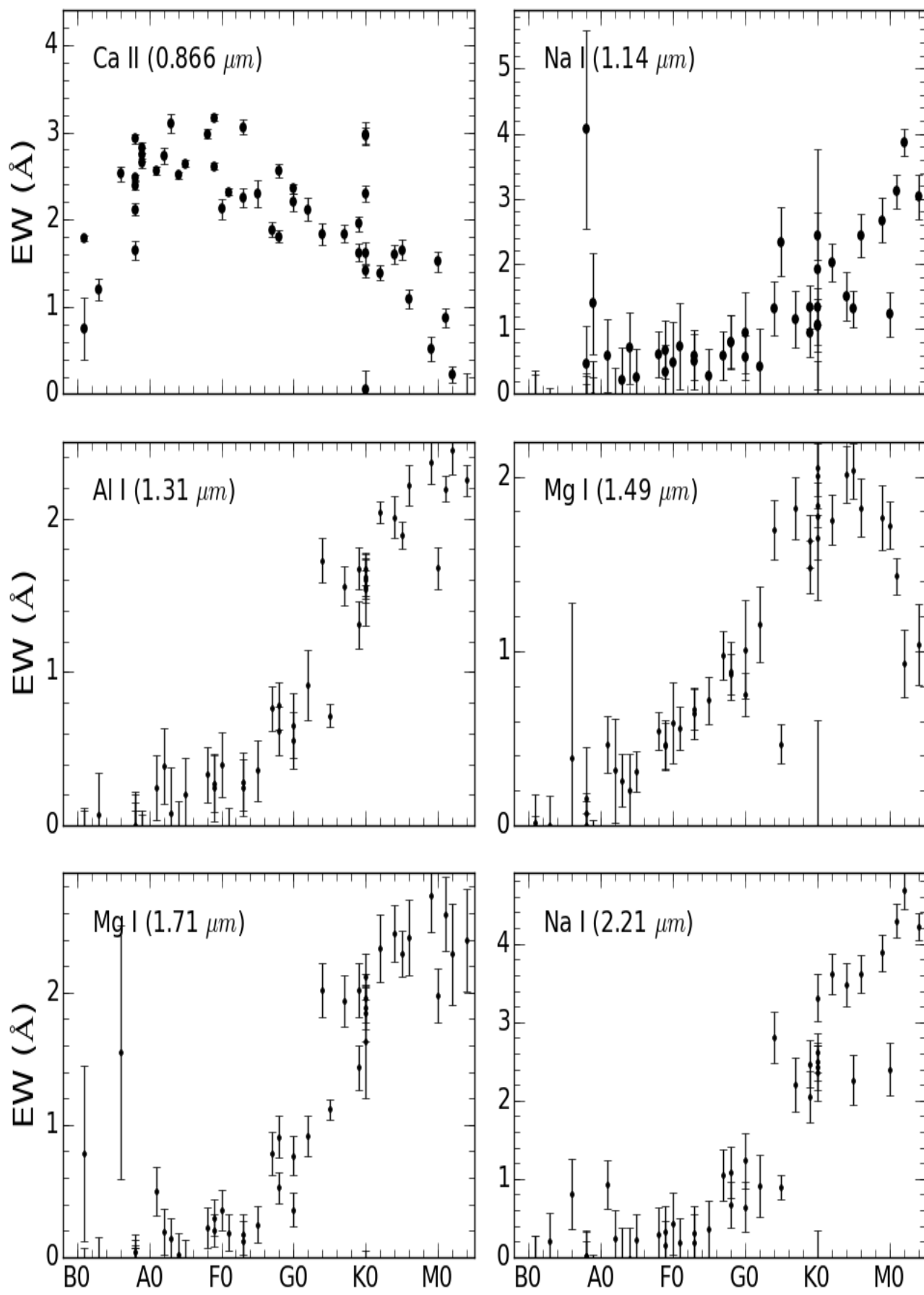












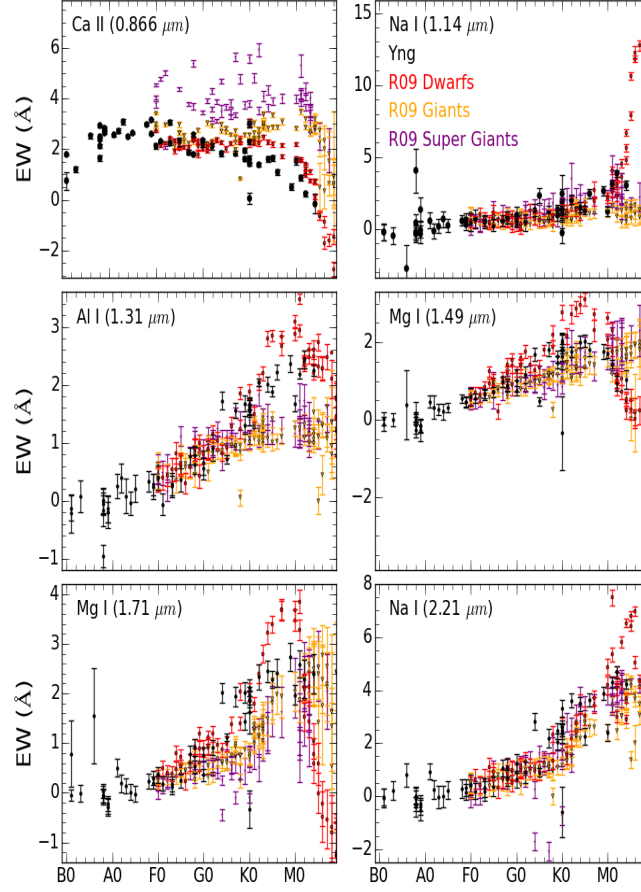


Fig. 14.— EWs of spectral features listed in Table 2 as a function of spectral type. Young stars are shown in black while R09 objects are in color. R09 stars were separated into three classes: dwarfs, giants, supergiants.

Table 3: EW values for spectral features listed in Table 2.

Object	Spectral Type	Ca II (0.866 μ m)	Na I (1.14 μ m)
HD 146266	A1V	2.56299927871 \pm 0.0505902823735	0.593124316048 \pm 0.55372199
HD 143472	A2V	2.72620156086 \pm 0.0890465928405	-0.124365182652 \pm 0.53092524
HD 145468	A3V	3.09676507059 \pm 0.105335208586	0.219012800854 \pm 0.49378354
HD 142424	A4V	2.50903380614 \pm 0.0418818508702	0.707624567334 \pm 0.54624929
HD 142097	A5V	2.63724671857 \pm 0.0387032039504	0.249643364628 \pm 0.43915267
HD 146899	A8V	2.98045841895 \pm 0.0563869594594	0.610106101858 \pm 0.35753207
HIP 73990	A9V	3.16901597018 \pm 0.0343419109672	0.332887913546 \pm 0.41442923
HD 147137	A9V	2.61193758312 \pm 0.0425581256529	0.674573918087 \pm 0.44666262
HIP 78933	B1V	1.79060453404 \pm 0.0292219340768	-0.225324048904 \pm 0.52465610
HD 144470	B1V	0.748607183674 \pm 0.353534583215	-0.189840080094 \pm 0.55912364
HD 138485	B3V	1.20021713217 \pm 0.123249228036	-0.459617243235 \pm 0.55869401
HD 147196	B6/B7Vn	2.52213176697 \pm 0.0903438021126	-2.6952099117 \pm 1.56138778
HIP 70753	B8V	2.39216215594 \pm 0.0467874269198	0.458962358336 \pm 0.58055595
HIP 77909	B8V	2.48348877896 \pm 0.0356986682689	-0.163081246205 \pm 0.49287346
HIP 79031	B8V	2.92313532374 \pm 0.0490276065772	-0.302182483479 \pm 0.45369845
HIP 78207	B8V	1.65203955311 \pm 0.108135748082	4.06821387941 \pm 1.52965998
HD 144661	B8V	2.11294061833 \pm 0.0699405826986	-0.30876422225 \pm 0.58216854
HIP 76633	B9V	2.64639933676 \pm 0.0571975714836	1.38932051895 \pm 0.787411059
HIP 79599	B9V	2.81912816636 \pm 0.0655007572171	-0.0537110373563 \pm 0.56113468
HD 143567	B9V	2.73921608292 \pm 0.0776068347864	-0.346482479213 \pm 0.61236750
HD 137130	F0V	2.1187101502 \pm 0.109996007908	0.478070933429 \pm 0.62315494
HIP 79369	F1V	2.31937736651 \pm 0.0441335792305	0.736814084079 \pm 0.65470201
HIP 82319	F3V	3.06056116029 \pm 0.0807534904999	0.596463524909 \pm 0.38397756
HD 146743	F3V	2.25045438173 \pm 0.103381509043	0.498907766341 \pm 0.42552977
HD 148153	F5V	2.29157107038 \pm 0.155742615121	0.269936653943 \pm 0.41998654
HIP 78977	F7V	1.88231995991 \pm 0.0851137562302	0.591071362265 \pm 0.37699486
HIP 71982	F8V	2.56060188894 \pm 0.0762131229772	0.798555225551 \pm 0.41701779
HD 142113	F8V	1.80715735375 \pm 0.065280032777	0.807408187185 \pm 0.41124682
HIP 61412	G0V	2.35262109221 \pm 0.0592524670013	0.563753159833 \pm 0.34277895
HD 148040	G0V	2.20053757099 \pm 0.101688995449	0.945525631363 \pm 0.62576932
HD 133748	G2V	2.11491753543 \pm 0.130076563777	0.434474969927 \pm 0.57501420
GSC 06793-00994	G4V	1.82943169529 \pm 0.122746870859	1.30690699955 \pm 0.415157159
HBC 649	G5V	-11.1492957606 \pm 0.138296074012	2.34180866524 \pm 0.527490396
GSC 06801-00186 (oldSpx)	K0IV(e)	1.61984274243 \pm 0.120570710423	1.0591344803 \pm 0.397727631
GSC 06801-00186	K0IV(e)	2.95767211472 \pm 0.089655798648	2.4310123804 \pm 0.358654746
GSC 06793-01406	G7V	1.83580456818 \pm 0.0985098972086	1.15935055549 \pm 0.435042431
GSC 06213-00306AB	G9V	1.62311949533 \pm 0.100699089538	1.33688888145 \pm 0.334508160
CD-25 11942	K0V	2.30203721938 \pm 0.0933113714974	1.05295210041 \pm 0.29715866
ScoPMS 214	K0 / K2IV(e)	1.40960995147 \pm 0.0646030261218	1.34696384811 \pm 0.285200757
HD 141813	K0 / K1III+	0.0522366059582 \pm 0.215325641091	1.90968185145 \pm 1.84440442
HD 14311	K0III	2.98372410744 \pm 0.130486483868	-0.235621959504 \pm 0.74817149
ScoPMS 44	K2 / K2IV(e)	1.3889969003 \pm 0.0833266847196	2.02571434786 \pm 0.290506093
GSC 06793-00797	K4V	1.60031113319 \pm 0.109051356026	1.5075712139 \pm 0.373198133

